Image of Intra-Unit-Cell Atom Appeared in Compton B(γ)-Function : "Compton Microscope"?

Bull. Coll. Med. Sci. Tohoku Univ. 6(1) : 11～22, 1997

Image of Intra-Unit-Cell Atom Appeared in Compton $B(r)$-Function : "Compton Microscope" ?

Teiji KOBAYASI

General Education, College of Medical Sciences, Tohoku University

コンプトン $B(r)$-関数に現れる単位胞内原子像 : "コンプトン顕微鏡" ?

小林悌二

東北大学医療技術短期大学部 一般教育

Key words : Atomic structure, Compton scattering, $B(r)$-function, Core-orthogonalization, Pseudopotential theory, Si, Ge

The $B(r)$-function for electrons in solid is a quantity defined by the Fourier inversion of the momentum density distribution function of the electron system in the field of Compton scattering. The valence electron $B(r)$-functions of semiconducting materials Si and Ge have been calculated by the pseudopotential theory containing the core-orthogonalization effect.

On the $B(r)$ contour map, a pattern reflecting position and size of an intra-unit-cell atom is observed. It is more sharply enhanced on the contour map of $\Delta B(r)$, the contribution of the core-orthogonalization to $B(r)$. It seems as if Compton scattering works as a microscope which detects local structure and size of the intra-unit cell atom ; "Compton microscope". The appearance of the image of atomic structure can be explained by the facts that the function $B(r)$ is the autocorrelation function of valence electron wave function. The image pattern originates from inter-core autocorrelation part of $B(r)$ through the core-orthogonalization terms in the wave function.

§ 1 Introduction

The Compton scattering of γ-ray or X-ray photon from electrons in solid provides us with information of electronic structure of the solid[1)~3)]. The Compton profile $J(q_z)$ is an experimentally observable function of the electron momentum component q_z in the direction of momentum transferred from the photon to the electron. It is directly connected with the density distribution of electron momentum $\boldsymbol{q}$[4)]. From the Compton profiles, we can derive various quantities on electronic structure in the momentum space. The most significant one is the distribution function of electron momentum density (EMD) $\rho(\boldsymbol{q})$[1)5)~8)]. The two-dimensional integration of EMD on momentum components q_x and q_y defines the Compton profile[4)] ;

$$J(q_z)=(1/2\pi)^2\int_{-\infty}^{\infty}dq_x\int_{-\infty}^{\infty}dq_y\rho(q_x,\ q_y,\ q_z). \tag{1}$$

The EMD function describes electron occupation of the momentum states and, therefore, plays a fundamental role in discussing electron behaviour in the momentum space by relating to the property of electronic bond in the solid.

The EMD function can be Fourier-transformed to a function of positional variable $\boldsymbol{r}$ in the real space. By introducing the Fourier inversion transform of EMD denoted usually as $B(\boldsymbol{r})$[7)~13)], the transformation is written as

$$\rho(\boldsymbol{q})=\int B(\boldsymbol{r})\exp(-i\boldsymbol{q}\cdot\boldsymbol{r})d^3\boldsymbol{r}, \tag{2}$$

$$B(\boldsymbol{r})=\sum_{q}\rho(\boldsymbol{q})\exp(i\boldsymbol{q}\cdot\boldsymbol{r})/N\Omega_0. \tag{3}$$

In the independent electron model, the EMD function $\rho(\boldsymbol{q})$ can be given by

$$\rho(\boldsymbol{q})=2\sum_{n}\sum_{k}\left|\int\Psi_{nk}(\boldsymbol{r})\exp(-i\boldsymbol{q}\cdot\boldsymbol{r})d^3\boldsymbol{r}/\sqrt{N\Omega_0}\right|^2, \tag{4}$$

where Ψ_{nk} is the wave function of an electron with wave vector $\boldsymbol{k}$ in the nth occupied band and $N\Omega_0$ is the volume of the crystal with N unit cells of volume Ω_0. Here, spin-state summation is simply substituted by the factor 2.

As was pointed out previously[7)8)14)15)], from a viewpoint of energy-band-theoretical calculation, especially, of pseudopotential (PP) theoretical one, it is far favorable in numerical accuracy to adopt an indirect derivation of EMD via $B(\boldsymbol{r})$-function based on eq. (2), not on eq. (4). In previous papers[7)8)], we have performed PP theoretical calculation of EMD's and Compton profiles for valence electron systems of semiconducting materials Si and Ge on the base of $B(\boldsymbol{r})$-function formalism. In the calculation, the core-orthogonalization (CO), namely, the orthogonalization of valence electron state to inner core-electron ones is taken into account in order to estimate and discuss the effect of this higher-order contribution to EMD's and Compton profiles quantitatively.

In the PP theory, the valence electron wave function is composed of two parts. The main part is the pseudo-wave function describing a relatively smooth-varying behaviour of the electron. The second part describes a spatially rapid oscillation of the valence electron near the atomic core[16)]. This atomic-electron-like behaviour is due to the fact that, passing the vicinity of atom, the valence electron recalls its native outermost atomic orbitals under a relatively stronger atomic potential near the core. Quantum mechanically the situation corresponds to the fact that the valence-electron eigen-state should be orthogonal to the eigen-states of inner core-electrons. The second part describes the CO terms in the wave function of the valence electron eigen-state. Effects of the CO terms on EMD and Compton profiles are discussed in detail in refs. 7 and 8.

The purpose of this paper is to discuss CO effects on the intermediate quantity $B(\boldsymbol{r})$ in the real space. In the course of calculation of EMD's and Compton profiles of Ge[7)] and Si[8)], it was found that the $B(\boldsymbol{r})$-function shows an interesting atom-like image of CO origin at the nearest core site around $\boldsymbol{r}=0$ in the [111] direction. The centre of the atom-like image is just on the real core site and the order of its spread is very similar to the physical core-radius. At more distant core sites such an image cannot be observed because of a rapid damping nature of the $B(\boldsymbol{r})$-function. Around the core site at $\boldsymbol{r}=0$, such an atom-like image cannot be observed because it is buried under the large peak of $B(\boldsymbol{r})$ with the peak value of uniform density of valence electrons. It seems as if Compton scattering works as a microscope detecting local structure and size of one of the intra-unit

cell atoms. In the diamond structure of Si or Ge, the unit cell contains two atoms.

In this paper, it will be shown that the appearance of the atom-like image can be explained by using the fact that the $B(\boldsymbol{r})$-function is represented[9)17)] in terms of the integration of the autocorrelation function of the electron wave function over the occupied electron states. Autocorrelation component due to the CO terms in the valence electron wave function plays an essential role.

In § 2 the method of calculation is outlined, and results are given in § 3. We will discuss properties of the atom-like image and its origin in § 4.

§ 2 Outline of Method of Calculation

In the PP framework, the valence electron wave function Ψ_{nk} orthogonalized to the inner core electron wave functions $\{\Psi_{ck}\}$ is given by[16)]

$$\Psi_{nk}(\boldsymbol{r})=N_{nk}[\Phi_{nk}(\boldsymbol{r})-\sum_c<\Psi_{ck}\mid\Phi_{nk}>\Psi_{ck}(\boldsymbol{r})], \tag{5}$$

where Φ_{nk} is the pseudo-part of the valence electron wave function, Ψ_{ck} is the wave function of the cth core electron state and N_{nk} is the normalization constant. We approximate Ψ_{ck} by the Bloch sum of the ionic core orbitals ϕ_c (tight-binding-limit approximation) as[16)]

$$\Psi_{ck}(\boldsymbol{r})=\sum_m\sum_{j=1}^{s}\phi_c(\boldsymbol{r}-\boldsymbol{R}_m-\boldsymbol{\tau}_j)\exp[i\boldsymbol{k}\cdot(\boldsymbol{R}_m+\boldsymbol{\tau}_j)]/\sqrt{sN}, \tag{6}$$

where $\boldsymbol{R}_m$ is the primitive translational vector pointing the mth unit cell in the crystal, and $\boldsymbol{\tau}_j$ is the non-primitive one within the unit cell with s atoms. For the diamond structure of Si and Ge, $s=2$. We define a plane wave expansion of Φ_{nk} as

$$\Phi_{nk}(\boldsymbol{r})=\sum_G C_{nk}^{\text{pseudo}}(\boldsymbol{G})\exp[i(\boldsymbol{k}+\boldsymbol{G})\cdot\boldsymbol{r}]/\sqrt{N\Omega_0}, \tag{7}$$

where $\boldsymbol{G}$ is the reciprocal lattice vector. By transforming $\phi_c(\boldsymbol{r})$ into $\phi_c(\boldsymbol{q})$, we will have

$$\Psi_{ck}(\boldsymbol{r})=\sum_G b_{ck}(\boldsymbol{G})\exp[i(\boldsymbol{k}+\boldsymbol{G})\cdot\boldsymbol{r}]/\sqrt{N\Omega_0}, \tag{8}$$

where

$$b_{ck}(\boldsymbol{G})=S(\boldsymbol{G})\phi_c(\boldsymbol{k}+\boldsymbol{G}), \tag{9}$$

in which

$$\phi_c(\boldsymbol{q})=\sqrt{s/\Omega_0}\int\phi_c(\boldsymbol{r})\exp(-i\boldsymbol{q}\cdot\boldsymbol{r})d^3\boldsymbol{r}, \tag{10}$$

and $S(\boldsymbol{G})$ is the structure factor

$$S(\boldsymbol{G})=\sum_{j=1}^{s}\exp(-i\boldsymbol{G}\cdot\boldsymbol{\tau}_j)/s. \tag{11}$$

Substitution of eqs. (7) and (8) into eq. (5) yields

$$\Psi_{nk}(\boldsymbol{r})=\sum_G C_{nk}(\boldsymbol{G})\exp[i(\boldsymbol{k}+\boldsymbol{G})\cdot\boldsymbol{r}]/\sqrt{N\Omega_0}, \tag{12}$$

$$C_{nk}(\boldsymbol{G})=N_{nk}[C_{nk}^{\text{pseudo}}(\boldsymbol{G})-\sum_c\sum_{G'}b_{ck}^*(\boldsymbol{G}')b_{ck}(\boldsymbol{G})C_{nk}^{\text{pseudo}}(\boldsymbol{G}')]. \tag{13}$$

Substituting eq. (12) into eq. (4) and its result into eq. (3), we will obtain the key expression for $B(\boldsymbol{r})$ as follows,

$$B(\boldsymbol{r})=2\sum_n\sum_k\sum_G\mid C_{nk}(\boldsymbol{G})\mid^2\exp[i(\boldsymbol{k}+\boldsymbol{G})\cdot\boldsymbol{r}]/N\Omega_0. \tag{14}$$

Contribution of the CO terms is defined by

$$\Delta B(\boldsymbol{r})=B(\boldsymbol{r})-B^{\text{pseudo}}(\boldsymbol{r}), \tag{15}$$

where $B^{\text{pseudo}}(\boldsymbol{r})$ is the $B(\boldsymbol{r})$-function of the pseudo valence electron system described by the pseudo wave functions with no CO terms, then is calculated by using $\{C_{nk}^{\text{pseudo}}(\boldsymbol{G})\}$ in eq. (14).

In a practical calculation, we will employ the crystal cubic harmonics expansion of $B(\boldsymbol{r})$[10)18)];

$$B(\boldsymbol{r})=\sum_l\sum_i B_{li}(r)K_l^i(\Omega_r),$$
$$B_{li}(r)=\int B(\boldsymbol{r})K_l^{i*}(\Omega_r)d\Omega_r, \tag{16}$$

where K_l^i is the crystal cubic harmonics of the lth order and i distinguishes the different independent harmonics of the same l. Details of the expansion method, the energy band calculation for obtaining a set of $\{C_{nk}^{\text{pseudo}}(\boldsymbol{G})\}$ and the determination of a set of $\{b_{ck}(\boldsymbol{G})\}$ for core orbitals are given in refs 7. and 8.

§ 3 Results

The functions $B(\boldsymbol{r})$, $B^{\text{pseudo}}(\boldsymbol{r})$ and $\Delta B(\boldsymbol{r})$ of Si with $1s$, $2s$ and $2p$ inner cores and of Ge with $1s$, $2s$, $2p$, $3s$, $3p$ and $3d$ inner cores are calculated. The atomic configuration of the diamond structure with tetrahedral bond is shown in Fig. 1(a). The cube shown in Fig. 1(a) has 4 times the volume of the unit cell. We have two atoms per unit cell. The intra-unit-cell atoms are, for example, atoms A and B in Fig. 1(a). Calculations in three dimensional zone of $\boldsymbol{r}$ are concentrated on the $(1\bar{1}0)$ plane containing the high-symmetry directions of [001], [112], [111], [221] and [110] shown in Fig. 1(b). The bond between the nearest neighbour atoms A and B is along the [111] direction. The bond length is $(\sqrt{3}/4)a$, where a is the lattice constant (a= 10.26327 a.u. for Si and a=10.67715 a.u. for Ge).

The expansion of $B(\boldsymbol{r})$ in terms of the crystal cubic harmonics is very convenient to draw the contour map of the $B(\boldsymbol{r})$-function. As described in refs. 7 and 8, a full convergence of the expansion was attained by inclusion of components of $l\leqq 22$, in which the first sixteen harmonics belonging to the Γ_1-representation of the O_h group are contained [l=0, 4, 6, 8, 10, 12 (i=1, 2), 14, 16 (i=1, 2), 18 (i=1, 2), 20 (i=1, 2) and 22 (i=1, 2)]. The term of l=0 corresponds to the spherical component, and the sum of terms over $l\geqq 4$ describes the anisotropic behaviour of $B(\boldsymbol{r})$.

Figures 2 and 3 show the contour maps of $B(\boldsymbol{r})$ of Si and Ge, respectively. In Figs. 2 and

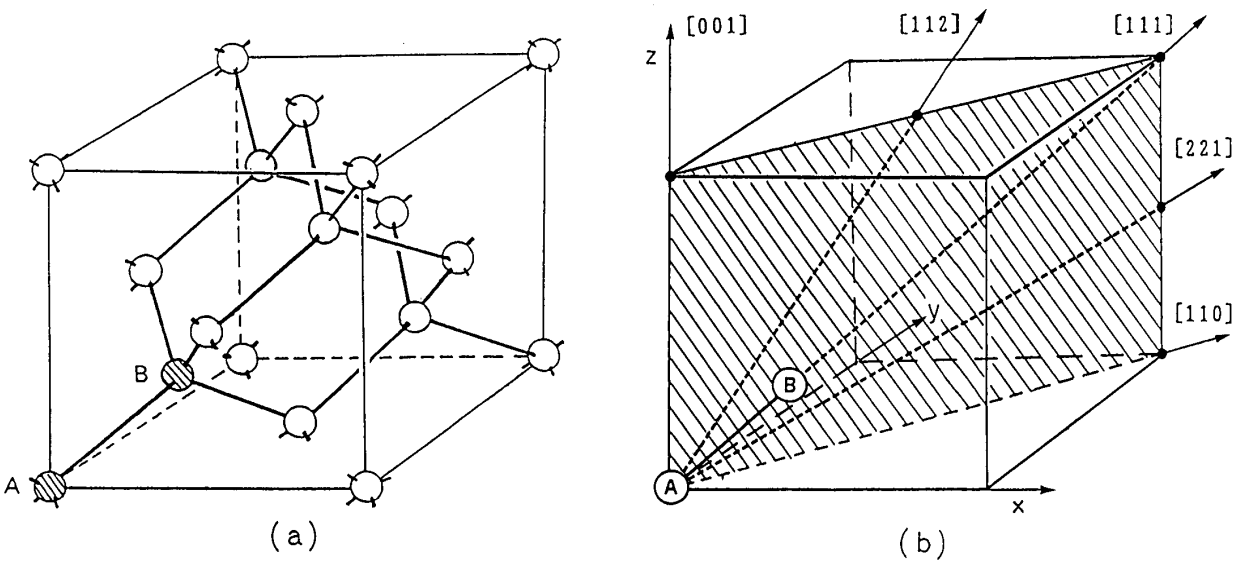

Fig. 1. (a) The atomic configuration of the diamond structure with tetrahedral bond. The side of cube is lattice constant a. The two intra-unit-cell atoms are indicated by A and B.
(b) The $(1\bar{1}0)$ plane containing the five high-symmetry directions. The bond between the nearest neighbour atoms A and B is along the [111] direction.

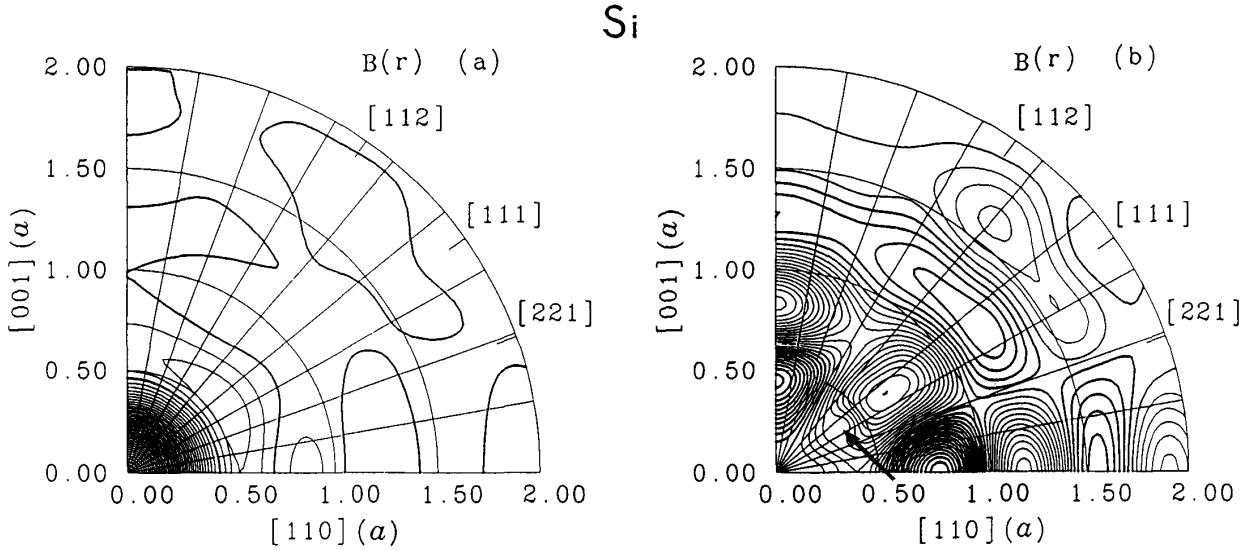

Fig. 2. Contour map of $B(\boldsymbol{r})$ of Si on the $(1\bar{1}0)$ plane: (a) Total $B(\boldsymbol{r})$ including the spherical component. (b) The Anisotropic part. A local pattern around the point $(1,1,1)a/4$ is arrowed.

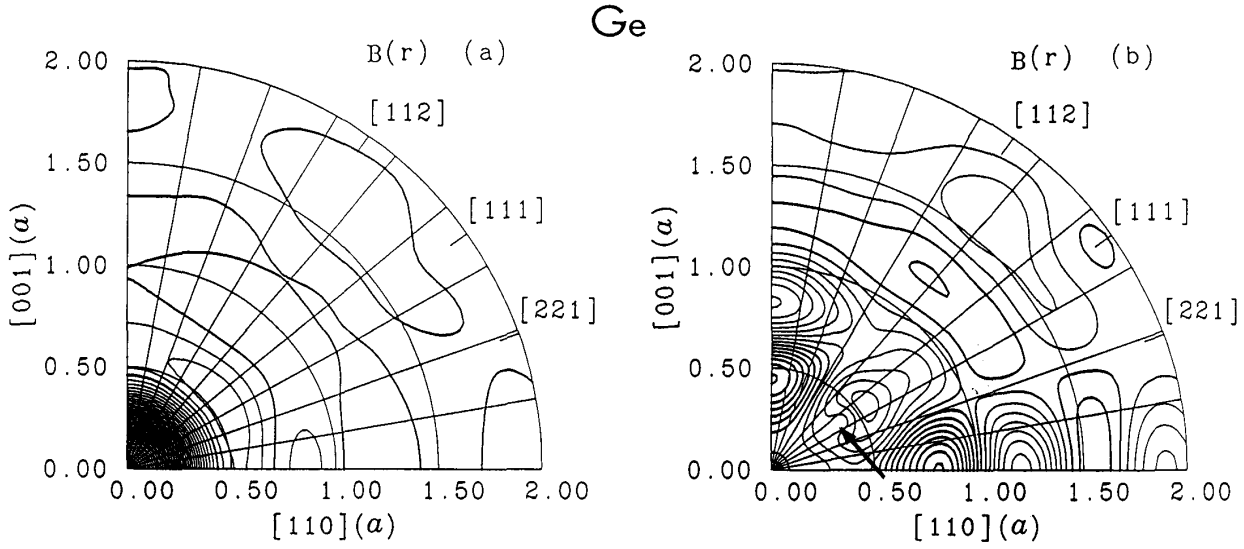

Fig. 3. Contour map of $B(\boldsymbol{r})$ of Ge on the $(1\bar{1}0)$ plane: (a) Total $B(\boldsymbol{r})$ including the spherical component. (b) The Anisotropic part. A local pattern around the point $(1,1,1)a/4$ is arrowed.

3, (a) shows the whole behaviour of $B(\boldsymbol{r})$ including the spherical component and (b) shows the anisotropic part. The distance parameter r is in units of a. The contour spacing in (a) is 0.1 and 0.01 in (b) in units of $2/\Omega_0$. Details of directional variation along the five directions are given in refs. 7 and 8. For the purpose of this paper, only the variation along the [111] direction is given. In Fig. 4 for Si and Fig. 5 for Ge, the sections of $B(\boldsymbol{r})$ and of its anisotropic part along the [111] direction are shown in (a) and (b), respectively.

Figures 6 and 7 show the contour maps of the CO contributions $\Delta B(\boldsymbol{r})$ of Si and Ge, respec-

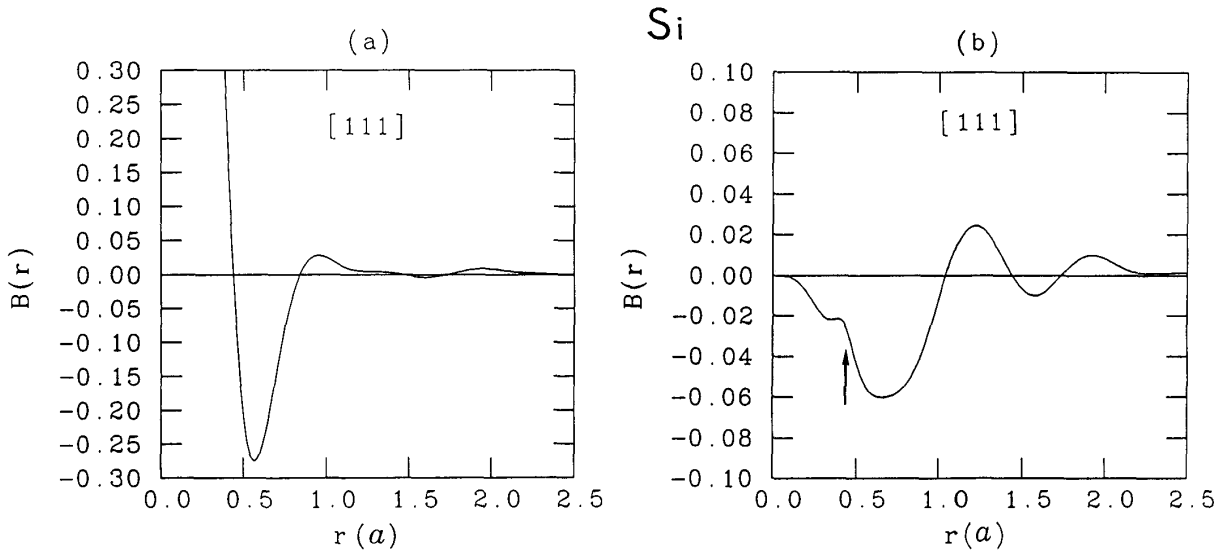

Fig. 4. Directional variation of $B(\boldsymbol{r})$ of Si along the [111] direction: (a) Total $B(\boldsymbol{r})$ including the spherical component. (b) The anisotropic part. The local pattern arrowed in Fig. 2(b) is observed as a shoulder structure.

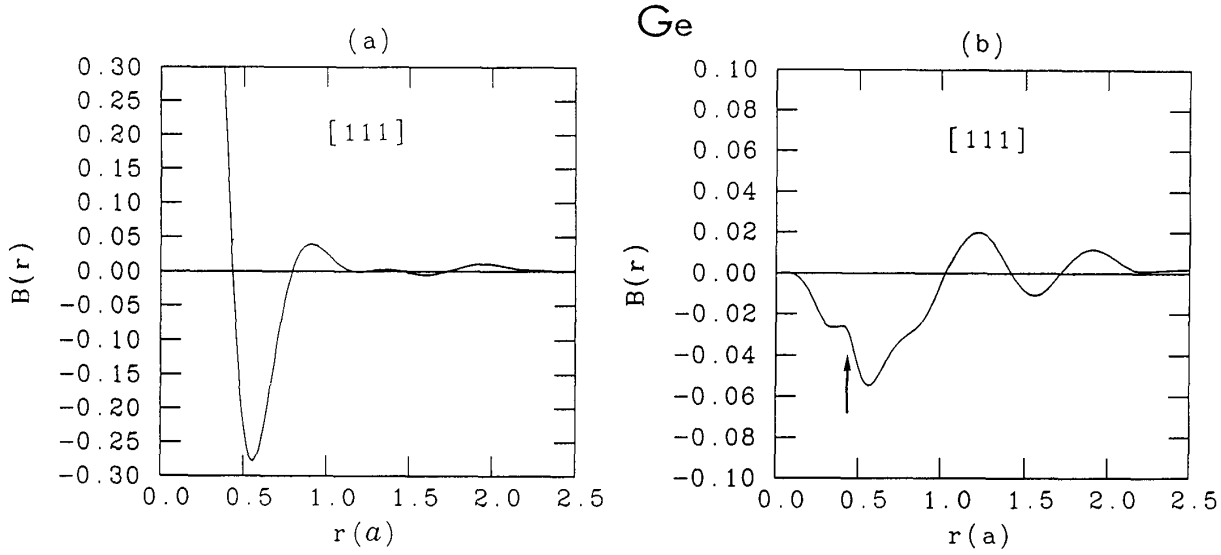

Fig. 5. Directional variation of $B(\boldsymbol{r})$ of Ge along the [111] direction: (a) Total $B(\boldsymbol{r})$ including the spherical component. (b) The anisotropic part. The local pattern arrowed in Fig. 3(b) is observed as a shoulder structure.

tively, in which the whole behaviour is presented in (a) and the anisotropic one is in (b). The contour spacing is 0.005. In Fig. 8 for Si and Fig. 9 for Ge, the sections of $\Delta B(\boldsymbol{r})$ and of the anisotropic part along the [111] direction are shown in (a) and (b), respectively.

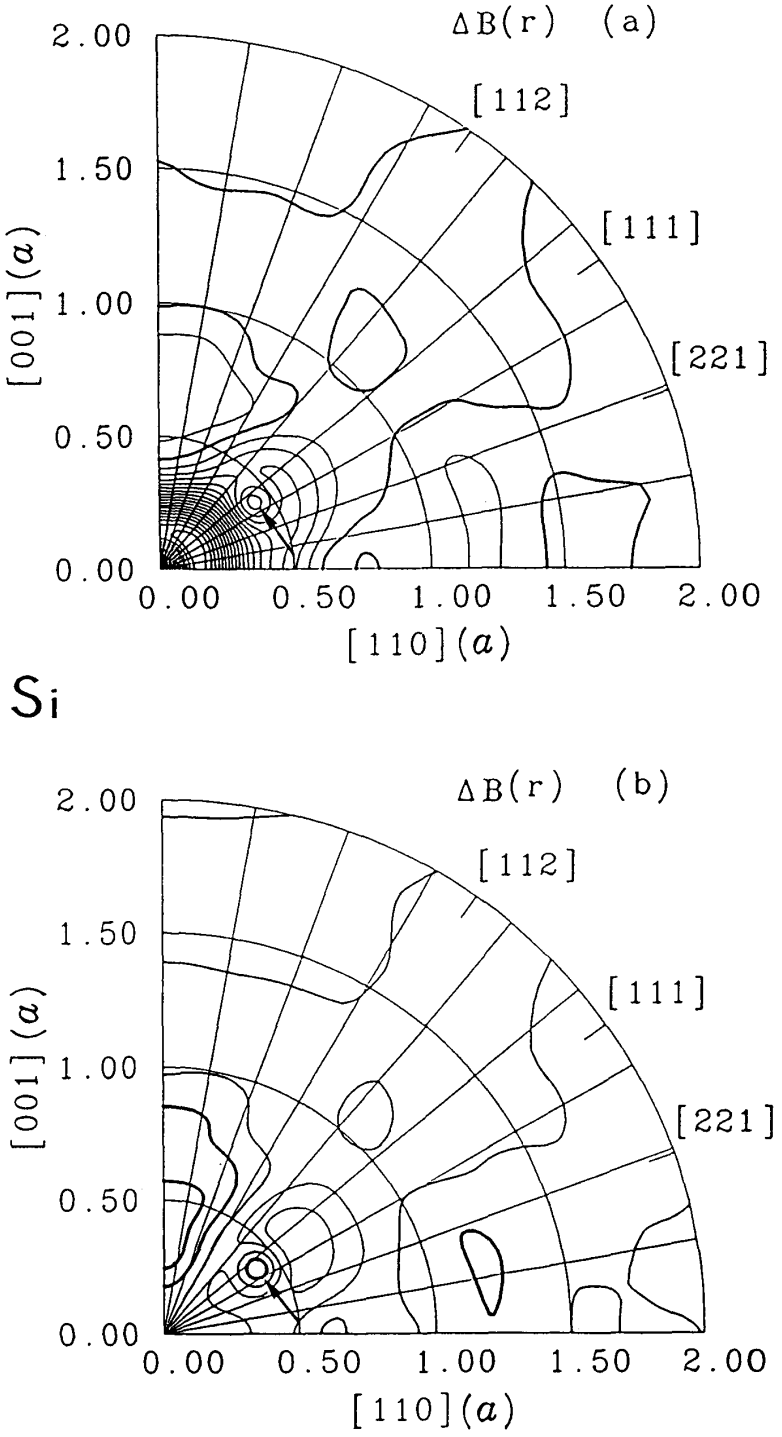

Fig. 6. Contour map of the CO contribution to $B(\boldsymbol{r})$, $\Delta B(\boldsymbol{r})$, of Si on the $(1\bar{1}0)$ plane: (a) Total $\Delta B(\boldsymbol{r})$ including the spherical component. (b) The anisotropic part.
The local pattern arrowed in Fig. 2(b) appears as a clear contour-circle centred on the point $(1, 1, 1)\,a/4$.

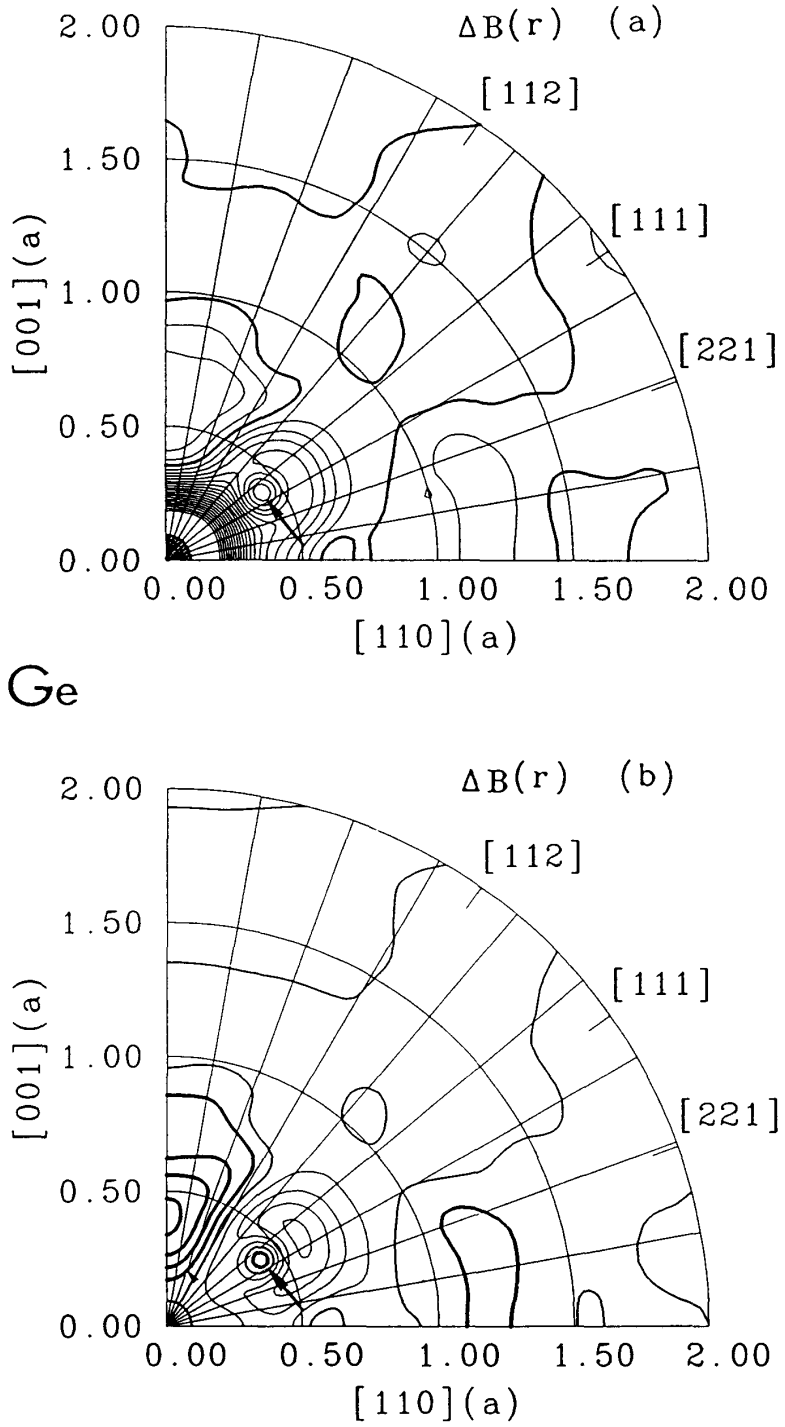

Fig. 7. Contour map of the CO contribution to $B(\boldsymbol{r})$, $\Delta B(\boldsymbol{r})$, of Ge on the $(1\bar{1}0)$ plane: (a) Total $\Delta B(\boldsymbol{r})$ including the spherical component. (b) The anisotropic part.
The local pattern arrowed in Fig. 3(b) appears as a clear contour-circle centred on the point $(1, 1, 1)\,a/4$.

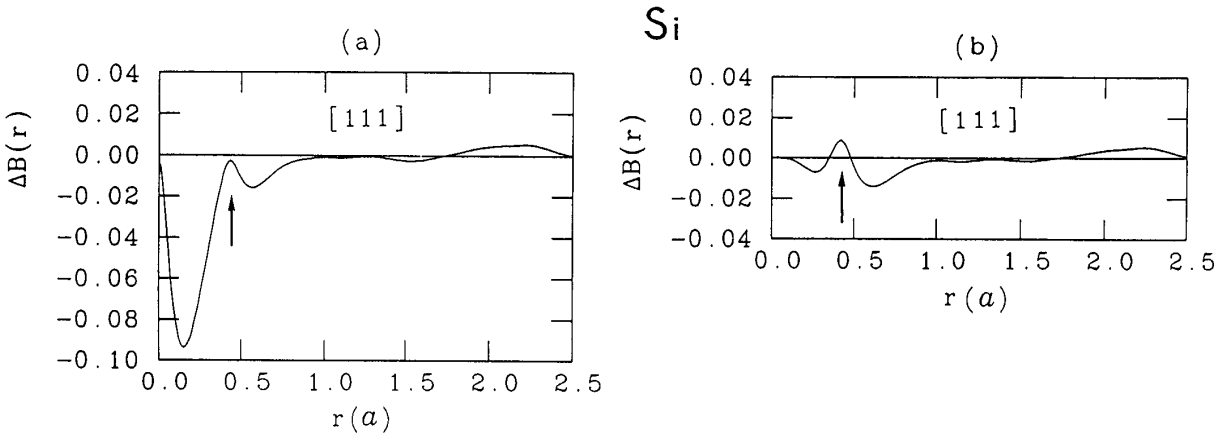

Fig. 8. Directional variation of $\Delta B(\boldsymbol{r})$ of Si along the [111] direction: (a) Total $\Delta B(\boldsymbol{r})$ including the spherical component. (b) The anisotropic part.
The contour-circle arrowed in Fig. 6 shows a sharp structure with a peak at $r=(\sqrt{3}/4)\,a$.

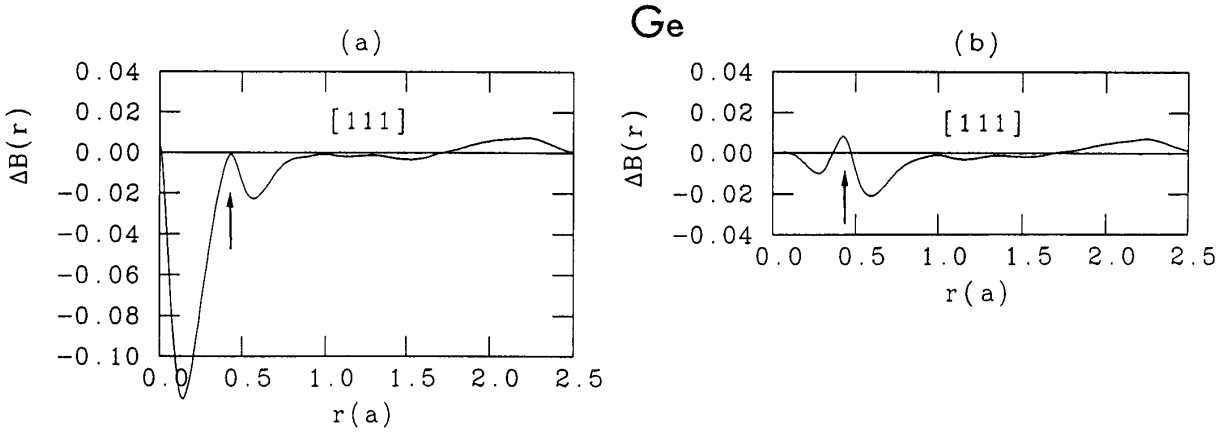

Fig. 9. Directional variation of $\Delta B(\boldsymbol{r})$ of Ge along the [111] direction: (a) Total $\Delta B(\boldsymbol{r})$ including the spherical component. (b) The anisotropic part.
The contour-circle arrowed in Fig. 7 shows a sharp structure with a peak at $r=(\sqrt{3}/4)\,a$.

§ 4 Discussion

As we can be seen from Figs. 2(a)~5(a), the $B(\boldsymbol{r})$-function has a large spherically symmetric part around $\boldsymbol{r}=0$ and it sharply damps outward. Anisotropic behaviour of $B(\boldsymbol{r})$ is enhanced in Figs. 2(b)~5(b) by subtraction of the spherical component from $B(\boldsymbol{r})$. We notice a local structure of contour being around the point at $\boldsymbol{r}=(1, 1, 1)a/4$ in the [111] direction, arrowed in Figs. 2(b)~5(b). The point is the atomic position of one of the two intra-unit-cell atoms shown in Fig. 1. If we put the atom A on $\boldsymbol{r}=(0, 0, 0)a$, the atom B is on $\boldsymbol{r}=(1, 1, 1)a/4$ by the bond length $(\sqrt{3}/4)a\,(=0.4330a)$ apart. The small local pattern is enhanced in the CO contribution to $B(\boldsymbol{r})$, $\Delta B(\boldsymbol{r})$, as Figs. 6~9 show. On the contour map of $\Delta B(\boldsymbol{r})$, the pattern appears clearly as a small circle centred on the point $(1, 1, 1)a/4$. In Figs. 8 and 9, it appears as a sharp peak at $r=0.433a$. The radius of the circle is roughly equal to $0.1a$. This is nearly equal to the physical core radius R_c; an example of estimated value[19] of R_c is $0.41\,\text{Å}=0.076a$ for Si^{4+}, and is $0.53\,\text{Å}=0.094a$ for Ge^{4+}. We can conclude that we observe a kind

of image of one of the intra-unit-cell atoms through the weak but characteristic pattern in $\Delta B(\boldsymbol{r})$ or in $B(\boldsymbol{r})$, as if we use the Compton scattering process as a microscope. In the following, the reason why an image of intra-unit-cell atom appears as a local pattern in $B(\boldsymbol{r})$ or in $\Delta B(\boldsymbol{r})$ is explained.

The $B(\boldsymbol{r})$-function can be written in the form of autocorrelation function of electron wave function integrated all over the occupied states as[9)17)]

$$B(\boldsymbol{r})=2\sum_n\sum_k\int \Psi^*_{nk}(\boldsymbol{r}')\Psi_{nk}(\boldsymbol{r}'+\boldsymbol{r})d^3\boldsymbol{r}'/N\Omega_0. \tag{17}$$

For the sake of simplicity we consider the one dimensional system of N atoms with one core state per atom. The pseudo valence electron is assumed to be in a single plane wave state.

The orthogonalized valence electron wave function is

$$\Psi_k(x) =N_k[\exp(ikx)/\sqrt{L}-\phi^*(k)\sum_m\exp(ikR_m) \times\phi(x-R_m)/\sqrt{N}], \tag{18}$$

where $\phi(x)$ is a core orbital function satisfying

$$\int\phi^*(x-R_m)\phi(x-R_n)dx=\delta_{R_m,R_n}, \tag{19}$$

$R_m=ma$ is the mth atom position (a: inter-atom spacing) in the system of length $L=Na$,

$$\phi(k)=\int\phi(x)\exp(-ikx)dx/\sqrt{a}, \tag{20}$$

and N_k is the normalization constant

$$N_k=1/[1-|\phi(k)|^2]^{1/2}. \tag{21}$$

All x-integrations are taken over the length of L.

After lengthy but exact derivation for $B(x)$ in the one dimensional system, namely,

$$B(x)=2\sum_k\int\Psi^*_k(x')\Psi_k(x'+x)dx'/L, \tag{22}$$

we obtain

$$B(x)=2\sum_k N_k^2\exp(ikx)[1-2|\phi(k)|^2]/L +2\sum_k N_k^2|\phi(k)|^2\sum_l\exp(ikR_l)\delta_{x,R_l}/L. \tag{23}$$

At the origin $x=0$, it is clearly seen that $B(x)$ is equal to the uniform density of electrons. The first term in the right side makes a bulk peak around $x=0$ and sharply damps outside, because the structure of k-integration over the occupied states is similar to that of

$$\int_{-G}^{G}\exp(ikx)dk =2\sin(Gx)/x=2Gj_0(Gx) \to 2\pi\delta(x)\quad(G\to\infty), \tag{24}$$

where j_0 is the 0th-order spherical Bessel function and $\delta(x)$ is Dirac's δ-function. The second term in the right side of eq. (23) comes from the autocorrelation within the CO terms and is of higher order contribution. It contains Kronecker's δ-function on the discrete atom position. At the atom position $x=R_l$, it gives the contribution of

$$2\sum_k N_k^2|\phi(k)|^2\sum_l\exp(ikR_l)/L$$

to $B(x)$ and more clearly to $\Delta B(x)$ as information of core. The value of this k-integral also damps rapidly with increase of x. As we have seen above, at $x=0$ the contribution of the second term is absorbed to reproduce the peak value of $B(0)$, the uniform density of electrons. These facts explain why the atom-like pattern appears and why it is limited on the atom sites close to the origin.

Experimentally, the EMD function $\rho(\boldsymbol{q})$ can be reconstructed from a set of Compton profiles $\{J(q_z)\}$, and $B(\boldsymbol{r})$ from $\rho(\boldsymbol{q})$. For one dimensional case, for example, along the [111] direction, more directly we can obtain $B(z)$ from $J(q_z)$. However, $\Delta B(\boldsymbol{r})$ itself is not an experimental product, as eq. (15) of its definition

shows. By combining experimental $B^{\text{pseudo}}(\boldsymbol{r})$ with theoretical $B(\boldsymbol{r})$, we will obtain semi-experimental $\Delta B(\boldsymbol{r})$. Many problems must be cleared to observe the fine CO effect experimentally. Problems are in experimental resolution, in procedure of various deconvolutions, in selection of a set of $\{J(q_z)\}$ in direction and q_z-size, in reconstruction procedure and so on. First of all, high resolusional power in experiments is most desirable. Test of observation of the CO effect may be an interesting problem in Silicon Project[20)21)].

References

1) Compton Scatterig, ed. Williams, B., McGrow-Hill, New York, 1977
2) Extended Abstracts of the 11th SAGAMORE Conference on Charge, Spin and Momentum Densities (held at Brest, France, August 7-12, 1994) ed. by Loupias, G. and Rabii, S., 1994
3) Informal Proceedings of the 2nd International Workshop on Compton Scattering and Fermiology (held at Tokyo, Japan, August 28-31, 1995) ed. by International Organizing and Program Committee of the Workshop, 1995
4) Platsman, P. and Tzoar, N.: Theory, Chap. 2 in ref. 1, pp. 28-42
5) Timms, D.N., Cooper, M.J., Holt, R.S. *et al.*: Compton Scattering Studies of the Valence Electron Density Distribution in GaAs, J. Phys.: Condens. Matter, **2**, 10517-10528, 1990
6) Nara, H., Kobayasi, T., Takegahara, K. *et al.*: Optimal Number of Directions in Reconstructing 3D Momentum Densities from Compton Profiles of Semiconductors, Comp. Mat. Sci., **2**, 366-374, 1994
7) Kobayasi, T., Nara, H., Timms, D.N. and Cooper, M.J.: Core-Orthogonalization Effects on the Momentum Density Distribution and the Compton Profile of Valence Electrons in Semiconductors, Bull. Coll. Med. Sci. Tohoku Univ., **4**, 93-104, 1995
8) Kobayasi, T.: Core-Orthogonalization Effect on the Compton Profiles of Valence Electrons in Si, Bull. Coll. Med. Sci. Tohoku Univ., **5**, 149-164, 1996
9) Cooper, M.J.: Compton Scattering and Electron Momentum Determination, Rep. Prog. Phys., **48**, 415-481, 1985
10) Mijnarends, P.E.: Reconstruction of Three-Dimensional Distributions, Chap. 10 in ref. 1, pp. 323-345
11) Pattison, P. and Williams, B.: Fermi Surface Parameters from Fourier Analysis of Compton Profiles, Solid State Commun., **20**, 585-588, 1976
12) Mueller, F.M.: Anisotropic Momentum Densities from Compton Profiles: Silicon, Phys. Rev., **B15**, 3039-3044, 1977
13) Kobayasi, T.: Fourier Inversion Formalism for the Calculation of Angular Correlation of Positron Annihilation Radiation of Semiconductors, Bull. Coll. Med. Sci. Tohoku Univ., **3**, 11-22, 1994
14) Nara, H., Shindo, K. and Kobayasi, T.: Pseudopotential Approach to Anisotropies of Compton-Profiles of Si and Ge, J. Phys. Soc. Jpn, **46**, 77-83, 1979
15) Nara, H., Kobayasi, T. and Shindo, K.: Anisotropies of Compton Profiles of Tetrahedrally Bonded Semiconductors, J. Phys. C: Solid State Phys., **17**, 3967-3974, 1984
16) Callaway, J.: Quantum Theory of the Solid, Part **A**, Academic Press, New York, 1974, Chap. 4 Energy Bands, pp. 242-351
17) Kobayasi, T.: Coupling of Positron Annihilation and Compton Scattering: A Proposal of a Positron Autocorrelation Function with Reduction of the Effect of Electron Distribution, Bull. Coll. Med. Sci. Tohoku Univ., **5**, 87-90, 1996
18) Mueller, F.M. and Priestley, M.G.: Inversion of Cubic de Haas-van Alphen Data, with an Application to Palladium, Phys. Rev., **148**, 638-643, 1966
19) Pauling, L.: The Nature of the Chemical Bond and the Structue of Molecules and Crystals (3rd ed.), Cornell University Press, Ithaca, 1960, Table 13-3 in Chap. 13, p. 514
20) Schülke, W.: The Status of the Silicon Project and Lessons Learnt from It: Experiment, pp.

97- 106 in ref. 3

Project, pp. 107-116 in ref. 3

21) Blaas, C.: A Theoretical Survey on the Si